Mineralogical Magazine, August 2018, Vol. 82(4), pp. 837–852

The crystal-chemistry of riebeckite, ideally $Na_2Fe_3^{2+}Fe_2^{3+}Si_8O_{22}(OH)_2$: a multi-technique study

UMBERTO SUSTA[1], GIANCARLO DELLA VENTURA[1,2,*], FRANK C. HAWTHORNE[3], YASSIR A. ABDU[3], MAXWELL C. DAY[3], BORIANA MIHAILOVA[4] AND ROBERTA OBERTI[5]

[1] Dipartimento di Scienze, Università di Roma Tre, I-00146 Roma, Italy
[2] INFN-LNF, I-00044 Frascati, Italy
[3] Department of Geological Sciences, University of Manitoba, Winnipeg, MB, R3T 2N2, Canada
[4] Mineralogisch-Petrographisches Institut, Universität Hamburg, Grindelallee 48, D-20146 Hamburg, Germany
[5] CNR-Istituto di Geoscienze e Georisorse, Sede di Pavia, I-27100 Pavia, Italy

[*Received 3 February 2017; Accepted 23 July 2017; Associate Editor: Sergey Krivovichev*]

Abstract

In this work we report on a complete crystal-chemical characterization of a near end-member riebeckite from Malawi, and use the available data to critically compare information obtained from different analytical methods. The sample occurs as well-formed and very large single crystals in pegmatitic rocks. Accurate site-populations were determined by combining single-crystal structure refinement and electron microprobe analysis (EMPA). The Fe^{3+}/Fe^{2+} ratio was obtained from Mössbauer spectroscopy. Lithium was quantified by Laser Ablation Inductively Coupled Plasma Mass Spectroscopy (LA-ICP-MS).

Fourier-Transform Infrared (FTIR) spectra, collected both on powders and single crystals, are presented and discussed. FTIR spectra in the NIR region are also presented for the first time for this amphibole. The FTIR data are compatible with complete local ordering of A cations close to F, and complete Fe^{2+}/Mg disorder at *M*(1,3). Polarized Raman-scattering data collected from single crystals confirm this conclusion. In addition, it was found that FTIR data collected on powders provide the best agreement with the site occupancies derived from chemical (EMPA and LA-ICP-MS) and crystal-chemical data, possibly because they do not depend on experimental issues such as orientation and polarization.

KEYWORDS: riebeckite, Malawi, EMP, Mössbauer, crystal-structure, FTIR and Raman spectroscopy.

Introduction

RIEBECKITE is a relatively common *C*2/*m* sodium amphibole with ideal composition $Na_2Fe_3^{2+}Fe_2^{3+}Si_8O_{22}(OH)_2$, and thus is the ferro-ferri- counterpart of glaucophane. Typically, riebeckite is found in peralkaline acid igneous rocks, high-grade schists and meta-ironstones (Deer *et al.*, 1997). The crystal structure of riebeckite was determined by Hawthorne (1978) on a F-rich sample from a granitic pegmatite in the Pikes Peak area of Colorado, USA. The specimen was also Li-bearing, a feature that was later recognized to be common in some sodium amphiboles with a significant Fe content and *A*-site occupancy (Hawthorne *et al.*, 1993, 1994). The synthesis of riebeckite and magnesio-riebeckite was reported by Ernst (1962), who found that the upper stability limit of riebeckite is 400°C lower than that of magnesio-riebeckite; F substitution for OH was found to increase the thermal stability of the amphibole, in agreement with the occurrence of F-rich riebeckite at magmatic conditions (Ernst, 1968). The asbestiform variety of riebeckite is known as 'crocidolite', or 'blue asbestos', and has been considered for decades an important industrial mineral because of its properties, including mechanical strength and flexibility, coupled to high chemical, thermal and mechanical durability (Zoltai, 1981). For these reasons, 'crocidolite' has

*E-mail: giancarlo.dellaventura@uniroma3.it
https://doi.org/10.1180/minmag.2017.081.064

been used in a large variety of technological applications. However it was later recognized, as with other asbestos minerals, as one of the most hazardous solid environmental pollutants (e.g. Gunter *et al.*, 2007), and banned from the market in 1973 in the USA (https://www.epa.gov/asbestos/us-federal-bans-asbestos).

Despite its importance in both petrology and environmental mineralogy, crystal-chemical studies on riebeckite are few: for example, complete reference data for well-characterized samples are not found in the literature. In this paper, we present for the first time a complete characterization of a near end-member riebeckite using a multi-technique approach. The sample studied was purchased from a mineral dealer. The host rock is an alkali pegmatite from Mt. Malosa, Zomba District, Malawi, and consists of centimetre-sized orthoclase with large (up to several cm long) amphibole and aegirine crystals. Associated minerals include rare-earth-element- and boron-rich minerals (e.g. Guastoni *et al.*, 2009, 2010). Due to the availability of many large single crystals, we were able to do a complete study of the sample, including micro-chemistry (EMPA and LA-ICP-MS), X-ray diffraction, Mössbauer spectroscopy, and vibrational spectroscopies performed on both single crystals (FTIR and Raman) and powders (FTIR).

Experimental methods

Single-crystal structure REFinement (SREF)

X-ray diffraction (XRD) data on a crystal 40 μm × 40 μm × 100 μm in size were collected at the University of Manitoba, Department of Geological Sciences (UM-DGS), using a Bruker D8 three-circle diffractometer equipped with a rotating-anode generator, multilayer optics, an APEX-II CCD detector and working with Mo*K*α radiation. A total of 16,415 intensities was collected up to 2θ = 60° using 2–4 s per frame (taken at steps of 0.2°) with a crystal-to-detector distance of 5 cm. Empirical absorption corrections (*SADABS*, Krause *et al.*, 2015) were applied, and multiple reflections were merged, resulting in 5346 reflections, corresponding to 1386 unique reflections in the *C2/m* space group (R_{int} = 1.2%). Unit-cell dimensions were obtained by least-squares refinement of the positions of 3950 reflections with $I > 10\sigma I$ in the same θ range and are reported in Table 1. The structure was refined with the program *SHELXTL* version 6.14 (Sheldrick, 2015) to an *R* index of 1.8%. All atoms but H were refined anisotropically using neutral-scattering factors. Atom coordinates and displacement parameters are reported in Tables 2 and 3, and selected interatomic distances are reported in Table 4. Detailed crystallographic information has been deposited as a cif with the Principal Editor of *Mineralogical Magazine* and is available as Supplementary material (see below).

TABLE 1. Unit-cell dimensions and crystallographic details for riebeckite from Malawi.

a (Å)	9.770(6)
b (Å)	18.080(10)
c (Å)	5.339(3)
β (°)	103.599(13)
V (Å^3)	916.6(9)
Crystal size (μm)	40 × 40 × 100
Radiation	Mo*K*α
No. reflections	16,415
No. Ewald reflections	5346
No. unique reflections	1386
R_1%	1.77
R_{int}%	1.19
w*R*%*	5.39
GoF	1.17
Z	2

*weight = $1/[\sigma^2(F_o^2) + (0.0298*P)^2 + 0.93*P]$, where $P = (\max(F_o^2, 0) + 2*F_c^2)/3$.

Microchemical analysis

The crystal used for XRD analysis was embedded in epoxy resin and polished for EMPA. WDS analyses were done using a Cameca SX-100 electron microprobe at UM-DGS; operating conditions were: 15 kV accelerating voltage, 20 nA beam current and 1 μm beam size. The standards used are (all *K*α lines): Na: albite; Si and Ca: diopside; F: fluoro-riebeckite; Mg: forsterite; Al: andalusite; K: orthoclase; Ti: titanite; Fe: fayalite; Mn: spessartine; Cl: tugtupite; V: VP_2O_7; Cr: chromite; and Zn: gahnite. Seventeen analytical points were measured on the sample.

The presence of Li was detected and quantified by Laser Ablation Induced Coupled Plasma Mass Spectroscopy (LA-ICP-MS) at UM-DGS on the same mount previously used for EMPA. A Merchantek New Wave UP-213 laser ablation device was used with a Nd:YAG source, wavelength = 213 nm, a 4 ns pulse width, a repetition rate of 10 Hz, a flat top beam, a 3–5 J/cm^2 fluence, a

https://doi.org/10.1180/minmag.2017.081.064 Published online by Cambridge University Press

TABLE 2. Atom coordinates, displacement parameters (Å^2), and refined site-scattering values (ss, in epfu) for riebeckite from Malawi.

Site	s.s.	*x*	*y*	*z*	U_{eq}
M(1)	49.87(8)	0	0.09097(2)	½	0.00789(11)
M(2)	50.44	0	0.18344(2)	0	0.00668(9)
M(3)	25.13(6)	0	0	0	0.00769(14)
M(4)	22.94(13)	0	0.27829(4)	½	0.0155(3)
T(1)		0.28130(3)	0.08586(2)	0.28993(6)	0.00703(9)
T(2)		0.29081(3)	0.17033(2)	0.80144(6)	0.00709(9)
A(*m*)	1.75(11)	0.045(2)	½	0.101(3)	0.055(6)
O(1)		0.11065(10)	0.09175(5)	0.2052(2)	0.0090(2)
O(2)		0.11978(9)	0.17278(5)	0.7371(2)	0.0096(2)
O(3)		0.11097(14)	0	0.7083(2)	0.0108(2)
H		0.2121(12)	0	0.773(7)	0.057(11)
O(4)		0.36653(9)	0.24871(5)	0.7996(2)	0.0110(2)
O(5)		0.34920(9)	0.12935(5)	0.0813(2)	0.0113(2)
O(6)		0.33978(9)	0.12117(5)	0.5756(2)	0.0108(2)
O(7)		0.32996(13)	0	0.2986(2)	0.0120(2)

epfu – electrons per formula unit.

beam size of 15–30 μm, a spot ablation mode, an ablation and a background time of 30 s. A Thermo Finnigan Element2 sector field ICP-MS was used with a plasma power of 1386 W, 15.8 l/min of cool gas, 0.86 l/min of auxiliary gas, 0.71 l/min of sample gas, 0.38 l/min of ablation carrier gas and a ThO/Th of 0.15%.

The analytical protocol consisted of a 10% mass window, 10 ms of sample time, a sample/peak of 10, an integration window of 10%, an EScan scanning type and an average integration type. Data reduction was done with the *Iolite 2.212* software (Paton, 2011), using a NIST SRM 610 standard reference material and SiO_2 as the internal standard.

Mössbauer spectroscopy

The Mössbauer spectrum was collected using a ^{57}Co(Rh) point source at UM-DGS. The sample was finely ground in acetone to avoid oxidation and then mixed with sugar. The powder was loaded into a Pb ring (with a 2 mm inner diameter) and covered with tape on both sides. Assuming a recoilless fraction of 0.7, the amount of sample corresponds to an absorber thickness of ~4 mg Fe/cm^2. The spectrometer was calibrated against α-Fe. Data were evaluated with the program *RECOIL* (Rancourt and Ping 1991; Rancourt *et al.*, 1993; Rancourt *et al.* 1996) using a classical full static Hamiltonian approach with Lorentzian-shaped doublets.

Fourier-transform infrared (FTIR) and Raman spectroscopies

Powder FTIR data were collected using a Nicolet iS50 spectrometer equipped with a KBr beam splitter and a DLATGS detector at UniRomaTre. A crystal fragment was finely ground, and two KBr pellets were prepared, one with a 5/150 mg (sample/KBr) for the OH-stretching region, and a second with 1/150 mg for the lower frequency region; digitized data were collected at a nominal resolution of 4 cm^{-1}. Single-crystal spectra were collected (at INFN-LNF, Frascati) using a Bruker Hyperion 3000 microscope equipped with a N_2-cooled MCT detector. The microscope was attached to a Vertex V70 optical bench, equipped with a KBr broadband beamsplitter and a Globar IR source. Nominal resolution was 4 cm^{-1} and 256 scans were accumulated for both spectrum and background. Samples were prepared as doubly polished sections.

Raman scattering data were acquired on cleavage sections using a Horiba Jobin-Yvon T64000 triple-monochromator spectrometer equipped with an Olympus BX41 confocal microscope and 50× objective. Data were collected in back-scattering geometry with a spectral resolution of 2 cm^{-1}. Two laser lines (λ = 514.532 and 488.0 nm) were used to verify the absence of photoluminescence peaks. Samples were oriented with the monoclinic *c* axis vertical under the microscope using their prismatic morphology. The laser beam was normal to the

https://doi.org/10.1180/minmag.2017.081.064 Published online by Cambridge University Press

TABLE 3. Anisotropic displacement parameters for riebeckite from Malawi.

Site	U^{11}	U^{22}	U^{33}	U^{23}	U^{13}	U^{12}
M(1)	0.0099(2)	0.0075(2)	0.0066(2)	–	0.00262(10)	–
M(2)	0.00701(13)	0.00633(13)	0.00684(13)	–	0.00191(9)	–
M(3)	0.0098(2)	0.0061(2)	0.0071(2)	–	0.00175(13)	–
M(4)	0.0188(5)	0.0128(4)	0.0187(5)	–	0.0122(3)	–
T(1)	0.0077(2)	0.0067(2)	0.0067(2)	−0.00019(10)	0.00167(11)	−0.00031(10)
T(2)	0.0077(2)	0.0072(2)	0.0065(2)	−0.00039(10)	0.00190(11)	−0.00103(10)
A(*m*)	0.072(12)	0.036(8)	0.078(11)	–	0.059(9)	–
O(1)	0.0081(4)	0.0097(4)	0.0090(4)	−0.0003(3)	0.0017(3)	−0.0003(3)
O(2)	0.0082(4)	0.0107(4)	0.0095(4)	−0.0009(3)	0.0017(3)	−0.0005(3)
O(3)	0.0111(6)	0.0103(6)	0.0110(5)	–	0.0026(5)	–
O(4)	0.0126(4)	0.0090(4)	0.0116(4)	−0.0009(3)	0.0034(3)	−0.0033(3)
O(5)	0.0099(4)	0.0143(4)	0.0098(4)	0.0038(3)	0.0025(3)	0.0000(3)
O(6)	0.0107(4)	0.0125(4)	0.0091(4)	−0.0033(3)	0.0022(3)	−0.0002(3)
O(7)	0.0120(6)	0.0072(5)	0.0163(6)	–	0.0026(4)	–

($\bar{1}10$) crystallographic plane, as verified by XRD; both parallel-polarized and cross-polarized patterns were measured. The measured Raman spectra were corrected for the Bose-Einstein population to remove the trivial temperature dependence of the intensities: $I_{\text{reduced}} = I_{\text{measured}}/(n(\omega, T)+1)$ with $n(\omega, T) = 1/(e^{\hbar\omega/k_B T} - 1)$, where k_B is the Boltzmann constant, ω is the wavenumber (in cm^{-1}), T is the temperature (K) and $\hbar = h/2\pi$ is the reduced Planck constant (Kuzmany, 2009). The temperature reduced spectra were then fitted with pseudo-Voigt functions to determine the peak positions, widths and integrated intensities.

Results

EMP analysis and crystal-chemical formula

The microchemical composition obtained as an average of 17 analytical points is given in Table 5. The crystal-chemical formula was calculated on the basis of 24 (O, OH, F or Cl) (Hawthorne and Oberti, 2007). The H_2O content was calculated based on the assumption that O(3) = (OH,F) = 2 atoms per formula unit (apfu). The FeO to Fe_2O_3 ratio was first estimated on the basis of electroneutrality requirements given that the number of A-group cations, and hence the total number of cations, can also be validated by SREF. Because LA-ICP-MS analysis of Li (averaged over six point analyses) gave only 71(12) ppm, Li was not included in the calculations.

Ferric vs. ferrous iron from Mössbauer spectroscopy

Initial evaluation of Mössbauer data was done using a model with one doublet for Fe^{3+} at *M*(2) and two doublets for Fe^{2+} at *M*(1) and *M*(3). The resulting amount of Fe^{3+} was 32.7% of total iron, corresponding to 1.5 apfu. However, the three-doublets model provided some inconsistencies with the formula reported in Table 5, e.g. a low Fe^{3+} content at *M*(2), a low Fe^{2+} content at *M*(1) (1.4 apfu) and a high Fe^{2+} content at *M*(3) (1.22 apfu). Thus a new model was chosen, which included Fe^{2+} at *M*(2) and an additional doublet corresponding to Fe^{2+} at *M*(4). This latter component was added because of a small but detectable shoulder at ~+1.7 mm/s, which could be resolved introducing a doublet with hyperfine parameters compatible with Fe^{2+} at *M*(4) (Hafner and Ghose, 1971). The resulting hyperfine parameters (Table 6)

https://doi.org/10.1180/minmag.2017.081.064 Published online by Cambridge University Press

TABLE 4. Selected interatomic distances (Å) angles (°) and polyhedral distortion for riebeckite from Malawi.

T(1)–O(1)	1.6252(14)	*T*(2)–O(2)	1.6254(14)	*M*(4)–O(2) ×2	2.4319(14)
T(1)–O(5)	1.6268(11)	*T*(2)–O(4)	1.5996(12)	*M*(4)–O(4) ×2	2.3407(13)
T(1)–O(6)	1.6279(12)	*T*(2)–O(5)	1.6451(11)	*M*(4)–O(5) ×2	2.8994(14)
T(1)–O(7)	1.6209(10)	*T*(2)–O(6)	1.6567(11)	*M*(4)–O(6) ×2	2.4928(14)
<*T*(1)–O>	1.625	<*T*(2)–O>	1.632	<*M*(4)–O>	2.541
TAV	0.76	TAV	11.44		
TQE	1.0002	TQE	1.0029		
M(1)–O(1) ×2	2.1087(13)	*M*(2)–O(1) ×2	2.1354(12)	*M*(3)–O(1) ×4	2.1362(12)
M(1)–O(2) ×2	2.1125(12)	*M*(2)–O(2) ×2	2.0371(12)	*M*(3)–O(3) ×2	2.096(2)
M(1)–O(3) ×2	2.1331(12)	*M*(2)–O(4) ×2	1.9219(11)	<*M*(3)–O>	2.123
<*M*(1)–O>	2.118	<*M*(2)–O>	2.031	OAV	72.17
OAV	50.81	OAV	39.09	OQE	1.0222
OQE	1.0153	OQE	1.0130		
O(5)–O(6)–O(5)	172.59(6)	*T*(1)–O(5)–*T*(2)	136.84(6)	*A*(*m*)–O(5) ×2	3.005(11)
O(6)–O(7)–O(6)	112.68(7)	*T*(1)–O(6)–*T*(2)	142.61(6)	*A*(*m*)–O(5) ×2	2.824(8)
		T(1)–O(7)–*T*(1)	146.54(9)	*A*(*m*)–O(6) ×2	2.852(13)
				A(*m*)–O(7)	2.559(14)
				A(*m*)–O(7)	3.15(2)
				A(*m*)–O(7)	2.700(14)
				<*A*(*m*)–O>	2.86

OAV and TAV = octahedral and tetrahedral angular variance (°^2); OQE and TQE = octahedral and tetrahedral quadratic elongation (dimensionless); Robinson *et al.* (1971).

TABLE 5. Microchemical analysis and unit formula of riebeckite from Malawi*.

Oxides	wt.%	Range	Ions	Apfu
SiO_2	51.52	52.25–50.25	Si^{4+}	7.97
Al_2O_3	0.71	0.20–1.57	Al^{3+}	0.03
TiO_2	0.04	0.01–0.08	Sum T	8.00
(FeO_{tot})	(35.75)	(35.49–36.18)	Al^{3+}	0.10
Fe_2O_3**	14.08		Ti^{4+}	0.01
FeO**	23.09		Fe^{3+}	1.64
MnO	0.37	0.25–0.47	Fe^{2+}	2.94
NiO	0.02	0.00–0.03	Mn^{2+}	0.05
ZnO	0.03	0.00–0.07	Mg^{2+}	0.26
MgO	1.12	0.64–1.53	Sum C	5.00
CaO	0.79	0.55–1.08	Fe^{2+}	0.05
Na_2O	6.26	9.95–6.42	Ca^{2+}	0.13
K_2O	0.19	0.10–0.29	Na^{+}	1.82
F	0.20	0.10–0.39	Sum B	2.00
H_2O	1.84		Na^{+}	0.06
O=F	–0.08		K^{+}	0.04
Sum	100.18		Sum A	0.10
			F^{-}	0.10
			OH^{-}	1.90
			Sum W	2.00

*Unit formula calculated on the basis of 24 O and 2 (OH,F); 17 point analysis were merged, and the analytical ranges indicate that the crystal is quite homogeneous.
**Calculated based on 0.10 A-group cations.

https://doi.org/10.1180/minmag.2017.081.064 Published online by Cambridge University Press

TABLE 6. Mössbauer site distribution parameters and site properties for riebeckite from Malawi as derived from the spectral resolution given in Fig. 1.

	$^{M(1)}Fe^{2+}$	$^{M(3)}Fe^{2+}$	$^{M(2)}Fe^{2+}$	$^{M(2)}Fe^{3+}$	$^{M(4)}Fe^{2+}$
IS (mm/s)	1.141(5)	1.140(8)	1.129(5)	0.400(5)	1.074(5)
QS (mm/s)	2.85(2)	2.47(2)	2.18(2)	0.453(8)	1.74(2)
Area %	39.0(0.1)	20.4(0.1)	7.3(0.1)	31.9(0.1)	1.4(0.1)

IS – isomer shift; QS – quadropole splitting.

are consistent with data from the literature (Ernst and Wai, 1970), with Fe^{2+} at the *M*(1) site having a quadrupole splitting of ~2.85 mm/s. Intermediate values of ~2.5 mm/s are found for Fe^{2+} at the *M*(3) site, whereas Fe^{2+} at the *M*(2) site has a quadrupole splitting of ~2.2 mm/s. The final model is shown in Fig. 1. The results of the fitting, including site proportions, are listed in Table 6.

The relative amounts of total Fe^{2+} and Fe^{3+} calculated from Mössbauer are: $Fe^{3+}_{tot} = 0.32$ and $Fe^{2+}_{tot} = 0.68$. These numbers are in good agreement with the estimated overall Fe^{3+} and Fe^{2+} contents obtained by EMPA + SREF analysis (0.36 and 0.64, respectively; Table 5).

Single-crystal structure refinement (SREF)

Site populations were derived by combining the refined site-scattering values and bond lengths obtained from SREF with the results from EMPA.

A site

EMPA and SREF results are consistent with a very low *A*-site occupancy in the riebeckite of this work. The *A*-site population by EMPA is 0.04 apfu K^+ and 0.06 apfu Na^+ (Table 6), and SREF shows that both cations are ordered at the *A*(*m*) site, which is shifted ~0.50 Å away from the centre of symmetry in the plane of the mirror. Comparison of the observed

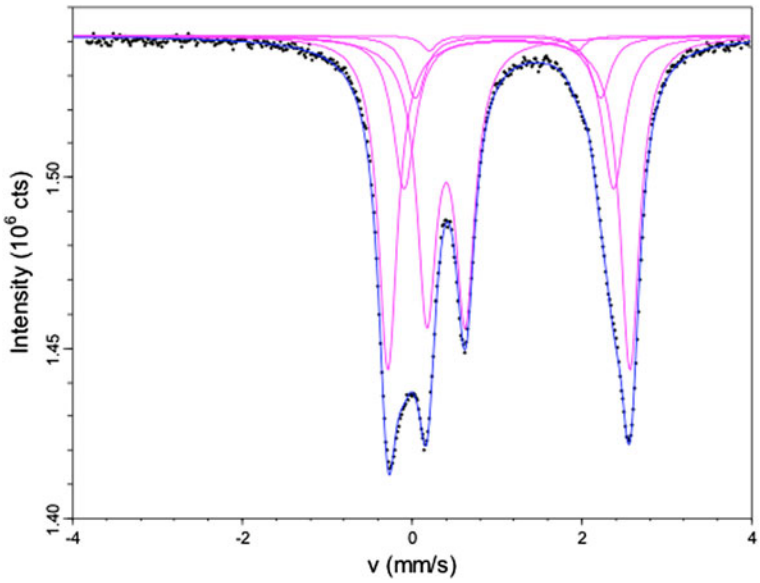

FIG. 1. Mössbauer spectrum of riebeckite from Malawi; spectral resolution based on the classical full static Hamiltonian approach with Lorentzian shaped doublets (see text for explanation).

https://doi.org/10.1180/minmag.2017.081.064 Published online by Cambridge University Press

(SREF) and calculated (from the unit formula) site-scattering values (Table 7) shows that the discrepancy, although within the standard deviation, is reasonable because of the very low occupancy and possible cation disorder.

T sites

According to the chemical analysis reported in Table 5, Si is 7.97 apfu, and hence $^{T(1)}Al^{3+}$ is 0.03 apfu, a result which is confirmed by the refined mean bond lengths at the *T*(1) and *T*(2) sites (Oberti *et al.*, 2007).

M(1,2,3) sites

In amphiboles with no significant oxo component, $^{C}(Mg^{2+}$, Fe^{2+} and $Mn^{2+})$ are distributed over the *M*(1,2,3) sites, whereas $^{C}(Fe^{3+}$, Al^{3+} and $Ti^{4+})$ are ordered at the *M*(2) site (Hawthorne and Oberti, 2007). Based on this assumption, and because the values of the refined site-scattering for the C cations are close to those calculated from the unit formula, the individual site populations of the *M*(1) site, which is likely to contain only two species (Mg and Fe), can be obtained from the refined site-scattering value: 26 $(Fe^{2+}) + 12\ (2 - Fe^{2+}) = 49.80$ epfu, which gives $^{M(1)}Fe^{2+} = 1.84$ apfu and $^{M(1)}Mg^{2+} = 0.16$ apfu. A similar calculation can be done for the *M*(3) site, where the available Mn^{2+} is likely to order based on current knowledge of the amphibole crystal-chemistry. The proposed site populations can be further validated by comparing the refined <*M*(1,2,3)–O> distances with those calculated by using the <cation–O> distances optimized for (OH,F)-amphiboles (Hawthorne and Oberti, 2007; Oberti *et al.*, 2007). The results are reported in Table 7.

M(4) site

A comparison of the refined site-scattering value with that calculated from the unit formula of Table 7 provides a reasonable agreement.

Comparison with Mössbauer results

A combination of the above data allows us to propose the following crystal-chemical formula: $^{A}(K_{0.06}Na_{0.04})^{B}(Na_{1.82}Ca_{0.13}Fe^{2+}_{0.05})^{C}[^{M(1)}(Fe^{2+}_{1.84}Mg^{2+}_{0.16})^{M(2)}(Fe^{2+}_{0.21}Mg^{2+}_{0.04}Fe^{3+}_{1.64}Al^{3+}_{0.10}Ti^{4+}_{0.01})\ ^{M(3)}(Fe^{2+}_{0.89}Mg^{2+}_{0.05}Mg^{2+}_{0.06})]^{T}(Si_{7.97}Al_{0.03})O_{22}\ ^{W}(OH_{1.9}F^{-}_{0.10})$; hence, the amphibole studied in this work is close to end-member riebeckite, ideally, $\square Na_2Fe^{2+}_3Fe^{3+}_2Si_8O_{22}(OH)_2$.

From Table 5 we can calculate the relative percentages (with respect to total Fe content) and compare them to those obtained by Mössbauer analysis: $^{M(4)}Fe^{2+} = 1.1$ *vs.* 1.4(0.1)%, $^{M(1)}Fe^{2+} = 39.7$ *vs.* 39.0(0.1)%, $^{M(3)}Fe^{2+} = 20.1$ *vs.* 20.4(0.1)%, $^{M(2)}Fe^{2+} = 3.7$ *vs.* 7.3(0.1)%, $^{M(2)}Fe^{3+} = 35.4$ *vs.* 31.9(0.1)%. They are significantly different only at the *M*(2) site. However, a rigid use of the Mössbauer results, would have provided a lower amount of Fe^{3+} and an higher amount of Fe^{2+} at the *M*(2) site, which would have worsened the agreement between observed and calculated mean bond lengths and, more important, would have generated a unit formula which is not electroneutral ($\Delta = -0.14$ charges).

TABLE 7. Final assigned site populations (apfu) and refined scattering values (epfu) for riebeckite from Malawi*.

Site	Site population (apfu)	Site scattering (epfu)		Mean bond lengths	
		obs	calc	obs	calc
T(1)	$3.97\ Si^{4+} + 0.03\ Al^{3+}$	56	55.97	1.625	1.620
T(2)	$4.00\ Si^{4+}$	56	56	1.632	
M(1)	$1.84\ Fe^{2+} + 0.16\ Mg^{2+}$	49.88(8)	49.76	2.118	2.120
M(2)	$0.21\ Fe^{2+} + 0.04\ Mg^{2+} + 1.64\ Fe^{3+} + 0.10\ Al^{3+} + 0.01\ Ti^{4+}$	50.44(9)	50.10	2.031	2.031
M(3)	$0.89\ Fe^{2+} + 0.05\ Mn^{2+} + 0.06\ Mg^{2+}$	25.13(6)	25.11	2.123	2.123
M(4)	$1.82\ Na^{+} + 0.13\ Ca^{2+} + 0.05\ Fe^{2+}$	22.94(13)	23.92		
A(*m*)	$0.06\ K^{+} + 0.04\ Na^{+}$	1.75(11)	1.58		
O(3)	$0.10\ F^{-} + 1.90\ (OH)^{-}$		28.10		

*Obs = from SREF; calc = from the site populations.

https://doi.org/10.1180/minmag.2017.081.064 Published online by Cambridge University Press

Vibrational spectroscopies (FTIR, Raman)

The hydroxyl modes

The OH-stretching FTIR spectrum collected on the KBr pellet is compared in Fig. 2 with the FTIR spectrum collected on a thin (26 μm) randomly oriented single-crystal section. The patterns are very similar and consist of three sharp peaks centred at 3650, 3635 and 3618 cm^{-1} in the powder spectrum, while being slightly shifted (by ~1 cm^{-1}) in the single-crystal spectrum. It is noteworthy that the powder spectrum has sharper peaks (full width at half maximum ≈7 cm^{-1}) than the single-crystal spectrum (FWHM ≈10 cm^{-1}). Asymmetry is observed in both spectra on the lower-wavenumber side of the main peak at 3618 cm^{-1}.

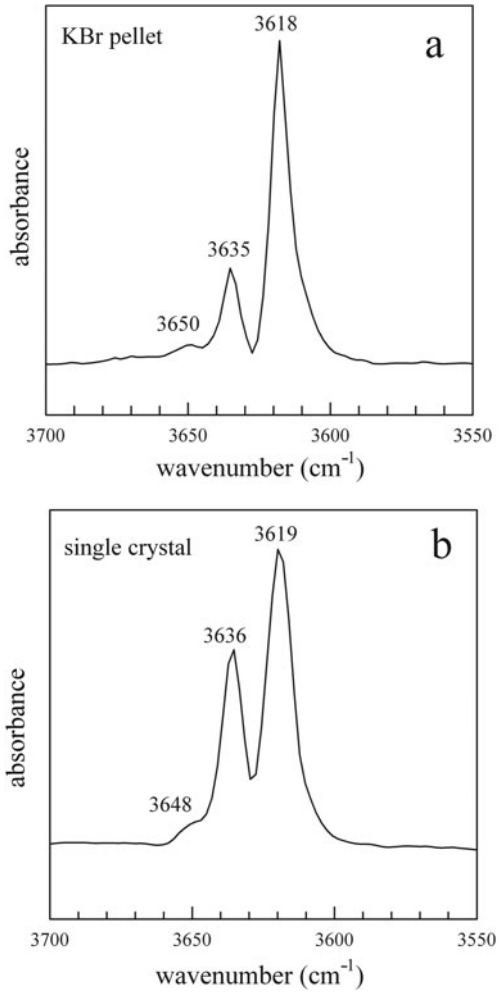

FIG. 2. FTIR OH-stretching spectra of riebeckite from Malawi, collected on (*a*) a KBr pellet and (*b*) on a 26 μm thick single crystal (unpolarized radiation).

The NIR spectrum collected on a thicker crystal fragment is shown in Fig. 3. FTIR data in the NIR region (4000–10000 cm^{-1}) for amphiboles are rare in the literature. Attempts to use the NIR spectra of actinolites or asbestos materials for remote-sensing applications have been published by Mustard (1992) and Lewis *et al.* (1996). According to these studies, bands due to the OH combination modes (stretching + libration) fall in the 4100–4500 cm^{-1} range, while the first overtone of the O–H stretching vibration is expected around 7100 cm^{-1}. The NIR spectrum of riebeckite from Malawi shows several peaks in the combination region, notably a multicomponent broad band centred at 4140 cm^{-1} and a triplet of bands at 4343, 4293 and 4266 cm^{-1}. The shape of these overlapping peaks is similar to that observed in the fundamental OH-stretching region; these three bands can, in fact, be assigned to the combination of the three stretching modes (ν_{OH}) observed in Fig. 2 with one OH libration (δ_{OH}) mode. Considering an average wavenumber ~4300 cm^{-1} for the combination triplet, and an average wavenumber ~3640 cm^{-1} for the fundamental mode(s), the wavenumber of the libration is ~650 cm^{-1}, in line with the few available data for the δ_{OH} mode in amphiboles (Ishida *et al.*, 2008). The splitting parameter between the three peaks is ~50 cm^{-1}, i.e. much larger that the splitting parameter between the corresponding three peaks in the fundamental region (~18 cm^{-1}; Fig. 2). The assignment of the broad absorption at 4140 cm^{-1} is not clear; it could be due either to a combination of the fundamental modes with a second OH libration at ~450 cm^{-1} or to an overtone of a T–O mode at ~1000 cm^{-1}. The first overtone of the O–H stretching ($2\cdot\nu_{OH}$) occurs as a relatively intense and sharp peak at 7065 cm^{-1} and two minor peaks at 7100 and 7134 cm^{-1}, respectively. The splitting parameters between these three components are constant and doubled with respect to those measured in the fundamental region (~34 cm^{-1} *vs.* ~17 cm^{-1}). Also, the overtone wavenumbers are far lower than twice the frequency of the corresponding fundamentals. The same behaviour has been observed for a variety of asbestos amphiboles, and it is a result of the significant anharmonicity of the O–H bond vibration (Lewis *et al.*, 1996). Further interesting features in the NIR spectrum reported in Fig. 3 are the very broad absorption extending from 5000 to 10,000 cm^{-1}, which peaks at ~8000 cm^{-1}, and the presence of an

https://doi.org/10.1180/minmag.2017.081.064 Published online by Cambridge University Press

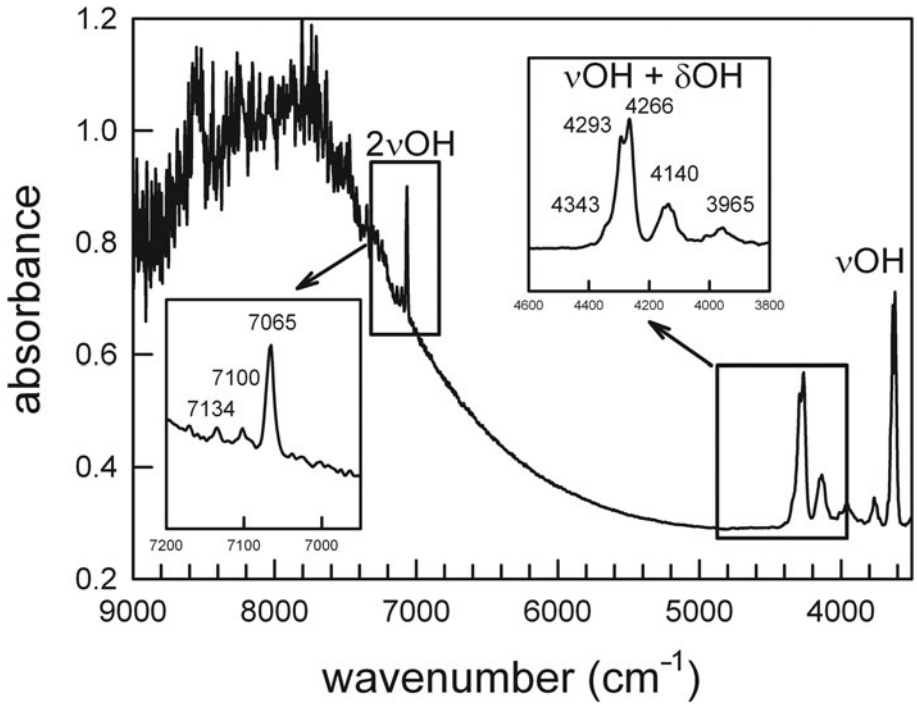

FIG. 3. The NIR spectrum of riebeckite from Malawi.

additional peak ~8500 cm^{-1}. Based on the literature data (i.e. Hawthorne, 1983; Mustard, 1992), this broad absorption should be related to electronic transitions and charge transfer between the Fe^{2+} and Fe^{3+} ions in the amphibole structure.

The Raman spectra recorded on the same sample are given in Fig. 4. Two spectra were collected with the crystal aligned (by morphology) with the **c** axis vertical with respect to the microscope view, and the polarization of the incident light (E_i) either parallel or perpendicular to the polarization of the scattered light (E_s) (royal blue and red, respectively in Fig. 4). Two further spectra were collected with the same polarization scheme but after rotating the crystal by 90° about the laser-beam direction (blue and pink, respectively, in Fig. 4). It is evident that both crystal orientation and the different polarization scheme have a strong effect on the spectrum. In particular, the OH-stretching signal (right side of Fig. 4) is maximized at parallel polarization ($E_i \parallel E_s$) and when $E_i \perp$ c, while the intensity vanishes for $E_i \perp E_s$. In any case, the $E_i \parallel E_s$ spectrum (royal blue in Fig. 4) is very similar to the FTIR spectrum, and consists of an intense peak at 3619 cm^{-1} and a weak peak at ~3640 cm^{-1}. Both peaks are rather sharp (FWHM ≈ 4 cm^{-1}) and have a symmetrical Lorentzian-type shape, thus indicating negligible chemical or structural disorder in the atomic environment of ^{W}OH in the areas probed.

The framework phonon region

The FTIR powder spectrum of the riebeckite studied in the low-frequency region (<1200 cm^{-1}) is shown in Fig. 5, and can be compared with the Raman spectra in the same region of Fig. 4. Raman spectroscopy has been used extensively to study amphiboles in the region of the framework phonon modes (Lazarev, 1972; Wang *et al.*, 1988*a*,*b*; Gillet *et al.*, 1989; Della Ventura *et al.*, 1991, 1993; Kloprogge *et al.*, 2001; Rinaudo *et al.*, 2004, 2006; Fornero *et al.*, 2008, among others). A collection of spectra for a large set of compositions was given by Apopei and Buzgar (2010). In contrast, FTIR data for the <1200 cm^{-1} region are relatively scarce; an analysis of IR spectra in this region was published by Andrut *et al.* (2000) for synthetic tremolite, Sr-substituted tremolite and richterite–tremolite solid solutions, and by Ishida *et al.* (2008) for synthetic

https://doi.org/10.1180/minmag.2017.081.064 Published online by Cambridge University Press

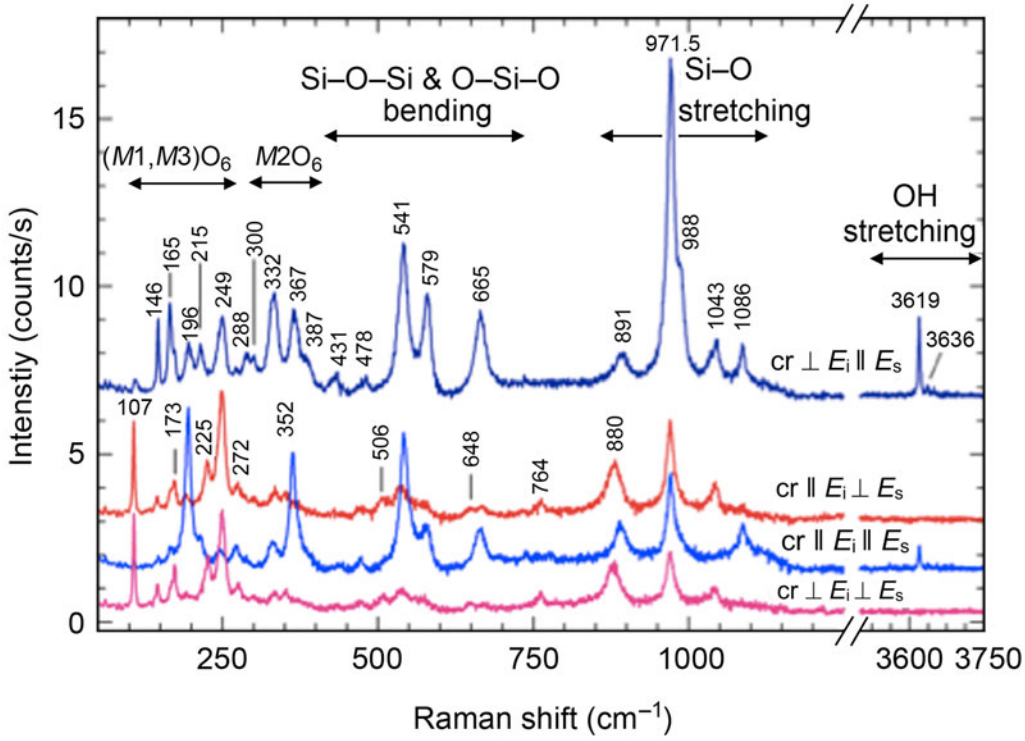

FIG. 4. Polarized Raman spectra of riebeckite from Malawi, measured in four different scattering geometries: cr designates the direction of the crystal prismatic axis, E_i and E_s denote the polarization of incident and scattered light. The peak positions are from spectral resolution. The band assignment is schematic and it is based on comparison with other amphiboles and other complex silicates (Apopei and Buzgar, 2010; Leissner *et al.*, 2015; Gasharova *et al.*, 1997).

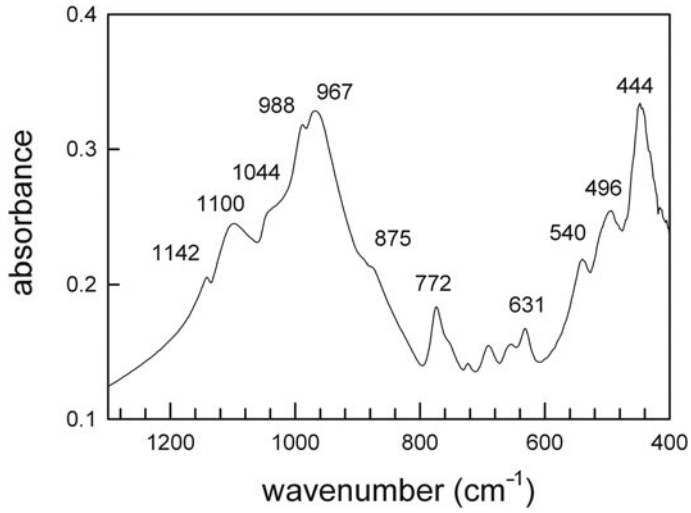

FIG. 5. The FTIR powder spectrum of riebeckite from Malawi in the low-frequency region.

https://doi.org/10.1180/minmag.2017.081.064 Published online by Cambridge University Press

calcium amphiboles; data for natural samples of various compositions have been given by Ishida (1989, 1990*a*,*b* and 1998).

According to the literature, Si–O bond-stretching vibrations occur in the 950–1130 cm^{-1} region and give rise to strong IR absorption in the spectrum of riebeckite (Fig. 5). The Raman spectrum shows two relatively weak bands at 1086 and 1043 (Fig. 4), which probably arise from Si–O stretchings involving bridging O atoms (O_{br}, shared between two TO_4), and a very intense peak (actually the most intense peak in the Raman pattern) at 972 cm^{-1} with an evident shoulder at 988 cm^{-1}. The 972 cm^{-1} peak most probably originates from Si–O bond-stretching involving non-bridging (O_{nbr}) oxygen atoms (Dowty, 1987). Amphiboles typically show their most intense Raman peak in the 680–650 cm^{-1} range, and the exact position of this peak has been proposed as a tool to identify the amphibole species, particularly when studying mineral fibres (e.g. Rinaudo *et al.*, 2004, 2006). In contrast, riebeckite exhibits an intermediate parallel polarized Raman peak in this range, at 665 cm^{-1} (Fig. 4) which is commonly assigned to Si–O–Si bending, also called the SiO_4-ring-breathing mode for silicates containing silicate rings, such as tourmaline, amphibole and layer silicates. Considering that all riebeckite spectra so far published (e.g. Apopei and Buzgar, 2010, Rinaudo *et al.*, 2004) show their most intense peak around 970 cm^{-1}, this type of pattern could possibly be used as a marker for this amphibole species. Furthermore, two parallel-polarized Raman peaks at 541 and 579 cm^{-1} even stronger than the peak at 665 cm^{-1} are observed for riebeckite. Such a feature is not common for amphiboles with predominantly divalent ions at the *M*(1,2,3) sites, but has been observed for pargasite (Leissner *et al.*, 2015). The phonon energy of the Raman peaks at 541 and 579 cm^{-1} matches the range of O–Si–O and Si–O–Si bending in silicates, and their stronger intensity for riebeckite might be related to the occurrence of both Fe^{2+} and Fe^{3+} at the *M*(1,2,3) sites and their influence on the TO_4 ring-modes. Further data are necessary to clarify this issue. The spectral range below 400 cm^{-1} should be dominated by MO_6 modes, with an additional contribution from TO_4 external modes and possible OH librations, following the general considerations for silicates (e.g. Lazarev, 1972 and Dowty, 1987; see also the correlation tables in Kloprogge *et al.*, 2001 and Apopei and Buzgar, 2010). In this region, riebeckite shows a complex pattern, consisting of several peaks at 367, 332, 249, 165 and 146 cm^{-1}, plus other minor features (Fig. 4). Most of these are intense for $E_i \parallel E_s$, whereas the 107 cm^{-1} peak has its maximum intensity for $E_i \perp E_s$.

Cation ordering in riebeckite from the OH-stretching spectra

Following previous spectroscopic literature on amphiboles with two divalent cations substituting at the O–H coordinated *M*(1,3) sites (e.g. Strens, 1966; Burns and Strens, 1966; Della Ventura, 1992; Della Ventura *et al.*, 1996, 1997, 1998, 1999, 2005, 2016; Hawthorne *et al.*, 2000; Iezzi *et al.*, 2004, 2005, Hawthorne and Della Ventura, 2007), and considering the crystal-chemistry of the sample studied, the peaks at 3618, 3636 and 3650 cm^{-1} in the FTIR spectra (Fig. 2) can be assigned to $Fe^{2+}Fe^{2+}Fe^{2+}$–OH–□–SiSi, $MgFe^{2+}Fe^{2+}$–OH–□–SiSi and $MgMgFe^{2+}$–OH–□–SiSi local arrangements, respectively. As discussed in previous papers (Wang *et al.*, 1988*a*,*b*; Leissner *et al.*, 2015; Della Ventura, 2017) the same number of bands occurs in the OH-stretching region of the FTIR and Raman spectra of amphiboles, as is also the case for the riebeckite of this work. However, a comparison of Figs 2 and 4 shows that the corresponding peaks have very different relative intensities (Table 8). In the Raman spectrum, the 3618 cm^{-1} peak due to the $Fe^{2+}Fe^{2+}Fe^{2+}$–OH configuration is by far the most intense, the 3636 cm^{-1} peak due to the $MgFe^{2+}Fe^{2}$

TABLE 8. Relative band (cm^{-1}) intensities (in %) from vibrational spectra*.

	A (3668)	B (3648)	C (3636)	D (3618)	$Fe^{2+}_{M(1,3)}$ (apfu)
FTIR powder	–	8	20	72	2.67
FTIR single crystal	–	4	38	58	2.44
Raman	–	–	18±4	82±4	2.82±0.14

*Results from Raman data are averaged over seven probed areas; uncertainties in the mean values are calculated from standard deviations.

https://doi.org/10.1180/minmag.2017.081.064 Published online by Cambridge University Press

$^{+}$–OH configuration is very weak, and the peak at 3648 cm^{-1}, due to the MgMgFe^{2+}–OH configuration is absent.

A further notable observation is that in both FTIR and Raman spectra, no band involving occupied *A*-site configurations (see also Della Ventura *et al.*, 2003) can be detected, although EMPA and SREF indicate that 0.08 A cations are present. This fact can be explained only when associating the *M*(1)*M*(1)*M*(3) configurations involving an occupied *A* site to F occurring at the O(3) site. This association is compatible with the crystal-chemical formula. In other words, all vibrational data suggest complete short-range order between $^{O(3)}$F and ^{A}(Na, K) in the amphibole studied. This conclusion is in agreement with SREF data. Ordering of A cations at the *A*(*m*) site in F-rich amphiboles is well known in amphiboles (Hawthorne *et al.*, 1996*a*), and is explained by positive Coulombic interactions given that *A*(*m*) is closer to the O(3) site occupied by F. It is now confirmed to be effective at very low F content.

Strens (1966) and Burns and Strens (1966) showed that when two divalent cations occur at the OH-coordinated *M*(1) and *M*(3) octahedra, the OH-stretching spectrum consists of four bands that are related to the four possible cation arrangements at the *M*(1,3) sites. Accordingly, the site occupancies of the two divalent cations can be related to the observed relative intensities of the four bands in the OH-spectrum (Law, 1976, Della Ventura *et al.*, 1996, Hawthorne *et al.*, 1996*b*, Della Ventura *et al.*, 1997, Iezzi *et al.*, 2005, Della Ventura *et al.*, 2005, 2016) provided that there is no variation in the molar absorptivity among the local configurations (Skogby and Rossman, 1991).

The spectra reported in Figs 2 and 4 were resolved using the *Peakfit*™ program by Jandel Scientific; for the single-crystal spectrum the background could be treated as linear, while for the powder spectrum a polynomial function was used to remove the broad absorption due to moisture in the pellet, which overlaps with the OH bands. We tried to minimize this effect by drying the mineral + KBr powder overnight at 110°C, but the broad absorption could not be significantly removed. All the bands were modelled as symmetric Gaussians (Della Ventura *et al.*, 1996); a minor additional peak at ~3610 cm^{-1} was necessary to take into account the asymmetry of the main band towards the lower frequency side. Because the corresponding Fe^{2+}Fe^{2+}Fe^{2+}-OH Raman peak collected from μm-sized spatial areas does not show an asymmetric shape, this asymmetry cannot be considered as an intrinsic feature of riebeckite, e.g. caused by phonon-electron interactions due to the presence of mixed-valence elements. Instead, it may be related to substitutional disorder at the NN *M*(1,3) or NNN *M*(2) and *M*(4) sites (e.g. Iezzi *et al.*, 2004, 2005) within the larger amount of sample probed by powder FTIR spectroscopy. In the first case, from the crystal-chemical formula given above, the only feasible candidate is Mn^{2+}; in the second case the only candidate is Ca at *M*(4). The presence of Fe^{3+} at *M*(1,3), coupled with O^{2-} at *W* might be also considered, however both the Mössbauer and SREF results rule out this hypothesis. The resulting relative integrated intensities, calculated by ignoring the 3610 cm^{-1} component, which has an area ~10% of the total absorption, are listed in Table 8, along with the relative Raman intensities arising from the OH stretching.

The data in Table 7 were treated using the equations of Burns and Strens (1966):

$$Mg^{2+}_{M(1,3)} = 3I^{o}_{A} + 2I^{o}_{B} + I^{o}_{C} \quad (1)$$
$$Fe^{2+}_{M(1,3)} = I^{o}_{B} + 2I^{o}_{C} + 3I^{o}_{D}$$

where I^{o}_{A},+ I^{o}_{B}, I^{o}_{C} and I^{o}_{D}, are the observed relative (integrated) intensities assigned respectively to the MgMgMg, MgMgFe^{2+}, MgFe^{2+}Fe^{2+} and Fe^{2+}Fe^{2+} Fe^{2+} local arrangements. The resulting Fe^{2+} contents at the *M*(1,3) sites from the FTIR (both powder and single-crystal) and Raman data are also listed in Table 8. Even considering the uncertainties associated with the estimation of the peak intensities, there are significant differences between the different methods; in fact FTIR powder spectroscopy yields a $^{M(1,3)}$Fe^{2+} content very similar to the value obtained by combining SREF + EMPA (Table 7); the $^{M(1,3)}$Fe^{2+} content obtained by single-crystal FTIR is significantly underestimated, due to the enhanced intensity of the C band with respect to the D band (Fig. 2 and Table 8). The different estimates may be partly due to probable inhomogeneities across the sample, that are averaged when analysing powders, and partly to problems related to the polarization of the O–H dipole, which are minimized in powders. The $^{M(1,3)}$Fe^{2+} content obtained by single-crystal Raman spectroscopy is slightly higher than the value obtained by powder FTIR spectroscopy but, within uncertainties, it still matches the site occupancy determined by combined SREF, EMPA and Mössbauer spectroscopy. In addition, it is worth noting that $^{M(1,3)}$Mn^{2+} in minor concentrations can hardly be distinguished from $^{M(1,3)}$Fe^{2+} via the OH stretching mode (e.g. Reece

https://doi.org/10.1180/minmag.2017.081.064 Published online by Cambridge University Press

et al., 2002; Oberti *et al.*, 2017), due to the very similar chemical characteristics of these elements (Leissner *et al.*, 2015); hence the more reliable values that one can obtain only on the basis of relative Raman intensities of OH stretching is $^{M(1,3)}$Mg and $^{M(1,3)}$Fe* = $^{M(1,3)}$(Fe^{2+} + Mn^{2+}).

From the relative band intensities in the FTIR spectra, information related to Fe^{2+}/Mg SRO can also be extracted (Della Ventura *et al.*, 1996). Assuming that Mg and Fe^{2+} are totally disordered at the *M*(1,3) sites, the relative band intensities can be calculated ($I^{C}_{B,C,D}$) following Strens (1966) and Law (1976) as:

$$I^{C}_{B} = x^{2}_{M(1)}\, y_{M(3)} + 2x_{M(1)}y_{M(1)}x_{M(3)} \quad (2)$$
$$I^{C}_{C} = y^{2}_{M(1)}x_{M(3)} + 2x_{M(1)}y_{M(1)}\, y_{M(3)}$$
$$I^{C}_{D} = y^{2}_{M(1)}\, y_{M(3)}$$

where $y_{M(1)}$ = Fe^{2+} at each of the two *M*(1) sites, $y_{M(3)}$ = Fe^{2+} at *M*(3), $x_{M(1)}$ = Mg at each of the two *M*(1) sites and $x_{M(3)}$ = Mg at *M*(3).

Substituting the site occupancies of Table 7 into equation 2, we obtain I^{C}_{B} = 2, I^{C}_{C} = 19 and I^{C}_{D} = 79. These values are in reasonable agreement with the observed relative intensities (FTIR powder data) given in Table 8, allowing us to conclude that there is complete Fe^{2+}/ Mg disorder over the *M*(1,3) sites in the riebeckite studied.

Conclusions

This work reports a multi-technique crystal-chemical study of a relatively common, but little studied Fe-rich sodium amphibole, riebeckite. A combination of refined site-scattering and Mössbauer data shows that trivalent cations are fully ordered at *M*(2), while OH-stretching spectroscopy (both FTIR and Raman) indicates complete short-range order of $^{O(3)}$F and ^{A}(Na, K). The Fe^{2+}/Mg composition at *M*(1,3) provided by powder FTIR is in excellent agreement with the site populations given by EMP and SREF, whereas single-crystal FTIR spectroscopy does not provide satisfactory results, possibly because FTIR powder data do not depend on features such as crystal orientation and beam polarization. This issue however needs to be investigated in detail on a larger set of amphiboles because vibrational spectroscopy can be important analytical tools for fibrous amphiboles of environmental/biomedical interest (e.g. Della Ventura, 2017). Single-crystal Raman spectroscopy only slightly overestimates the content of Fe^{2+} at *M*(1,3), but within the experimental uncertainty (5%); therefore, this method is a reliable tool for a non-destructive crystal-chemical analysis.

Acknowledgements

P. Leverett, W. Maresch and an anonymous referee provided careful reviews of the manuscript. G. Redhammer (Salzburg) helped with the interpretation of the Mössbauer spectrum and T. Malcherek (Hamburg) helped with the XRD orientation of the sample used for Raman measurements. Part of this work was done during the stay of U.S. at the Department of Geological Science (UM, Winnipeg) financed by a PhD grant from Roma Tre University.

Supplementary material

To view supplementary material for this article, please visit https://doi.org/10.1180/minmag.2017.081.064

References

Andrut, M., Gottschalk, M., Melzer, S. and Najorka, J. (2000) Lattice vibrational modes in synthetic tremolite-Sr-tremolite and tremolite–richterite solid solutions. *Physics and Chemistry of Minerals*, **27**, 301–309.

Apopei, A.I. and Buzgar, N. (2010) The Raman study of amphiboles. *Analele Ştiinţifice ale Universităţii "Al. I. Cuza" Iaşi, Geologie*, **56**, 57–83.

Burns, P.C. and Strens, R.G.J. (1966) Infrared study of the hydroxyl bonds in clinoamphiboles. *Science*, **153**, 890–892.

Deer, W.A., Howie, R.A. and Zussman, J. (1997) *Rock-forming Minerals, Vol 2B, Double-Chain Silicates*, *2nd ed*. 764 p., Geological Society, London.

Della Ventura, G. (1992) Recent developments in the synthesis and characterization of amphiboles. Synthesis and crystal-chemistry of richterites. *Trends in Mineralogy*, **1**, 153–192.

Della Ventura, G. (2017) The analysis of asbestos minerals using vibrational spectroscopies (FTIR, Raman): crystal-chemistry, identification and environmental applications. Pp. 135–169 in: *Mineral fibres: Crystal chemistry, chemical-physical properties, biological interaction and toxicity* (A.F. Gualtieri, editor). EMU notes in Mineralogy, **Vol. 18**.

Della Ventura, G., Robert, J.L. and Bény, J.M. (1991) Tetrahedrally coordinated Ti^{4+} in synthetic Ti rich potassic richterite: Evidence from XRD, FTIR and Raman studies. *American Mineralogist*, **76**, 1134–1140.

Della Ventura, G., Robert, J.L., Bény, J.M., Raudsepp, M. and Hawthorne, F.C. (1993) The OH-F substitution in

https://doi.org/10.1180/minmag.2017.081.064 Published online by Cambridge University Press

Ti-rich potassium-richterites: Rietveld structure refinement and FTIR and microRaman spectroscopic studies of synthetic amphiboles in the system K_2O-Na_2O-CaO-MgO-SiO_2-TiO_2-H_2O-HF. *American Mineralogist*, **78**, 980–987.

Della Ventura, G., Robert, J.L. and Hawthorne, F.C. (1996) Infrared spectroscopy of synthetic (Ni,Mg,Co)-potassium-richterite. *Geochimica and Cosmochimica Acta*, **5**, 55–63.

Della Ventura, G., Robert, J.L., Raudsepp, M., Hawthorne, F.C. and Welch, M. (1997) Site occupancies in synthetic monoclinic amphiboles: Rietveld structure-refinement and infrared spectroscopy of (nickel, magnesium, cobalt)-richterite. *American Mineralogist*, **82**, 291–301.

Della Ventura, G., Robert, J.L., Hawthorne, F.C., Raudsepp, M. and Welch, M.D. (1998) Contrasting $^{[6]}$Al ordering in synthetic Mg- and Co-pargasite. *Canadian Mineralogist*, **36**, 1237–1244.

Della Ventura, G., Hawthorne, F.C., Robert, J.L., Delbove, F., Welch, M.F. and Raudsepp, M. (1999) Short-range order of cations in synthetic amphiboles along the richterite-pargasite join. *European Journal of Mineralogy*, **11**, 79–94.

Della Ventura, G., Hawthorne, F.C., Robert, J.L. and Iezzi, G. (2003) Synthesis and infrared spectroscopy of amphiboles along the tremolite – pargasite join. *European Journal of Mineralogy*, **15**, 341–347.

Della Ventura, G., Redhammer, G.J., Iezzi, G., Hawthorne, Papin, A. and Robert, J.L. (2005) A Mössbauer and FTIR study of synthetic amphiboles along the magnesioriebeckite – ferri-clinoholmquistite join. *Physics and Chemistry of Minerals*, **32**, 103–113.

Della Ventura, G., Redhammer, G., Robert, J.L., Sergent, J., Iezzi, G. and Cavallo, A. (2016) Crystal-chemistry of synthetic amphiboles along the join richterite - ferro-richterite: a combined spectroscopic (FTIR, Mössbauer), XRPD and microchemical study. *Canadian Mineralogist*, **54**, 97–114.

Dowty, E. (1987) Vibrational interactions of tetrahedra in silicate glasses and crystals: I. calculations on ideal silicate aluminate-germanate structural units. *Physics and Chemistry of Minerals*, **14**, 80–93.

Ernst, W.G. (1962) Synthesis, stability relations and occurrence of riebeckite and riebeckite – arfvedsonite solid solutions. *Journal of Geology*, **70**, 689–736.

Ernst, W.G. (1968) *Amphiboles*. Springer-Verlag, Berlin.

Ernst, W.G. and Wai, M. (1970) Mössbauer, infrared, X-ray and optical study of cation ordering and dehydrogenation in natural and heat-treated sodic amphiboles. *American Mineralogist*, **55**, 1226–1258.

Fornero, E., Allegrina, M., Rinaudo, C., Mazziotti-Tagliani, S. and Gianfagna, A. (2008) Micro-Raman spectroscopy applied on oriented crystals of fluoro-edenite amphibole. *Periodico di Mineralogia*, **77**, 2–14.

Gasharova, B., Mihailova, B. and Konstantinov, L. (1997) Raman spectra of various types of tourmalines. *European Journal of Mineralogy*, **9**, 935–940.

Gillet, P., Reynard, B. and Tequi, C. (1989) Thermodynamic properties of glaucophane. New data from calorimetric and spectroscopic measurements. *Physics and Chemistry of Minerals*, **16**, 659–667.

Guastoni, A., Nestola, F. and Giaretta, A. (2009) Mineral chemistry and alteration of rare earth element (REE) carbonates from alkaline pegmatites of Mount Malosa, Malawi. *American Mineralogist*, **94**, 1216–1222.

Guastoni, A., Kondo, D. and Nestola, F. (2010) Bastnäsite-(Ce) and Parisite-(Ce) from Mt. Malosa, Malawi. *Gems & Gemology*, **46**, 42–46.

Gunter, M.E., Belluso, E. and Mottana, A. (2007) Amphiboles: Environmental and health concerns. Pp. 453–516 in: *Amphiboles: Crystal Chemistry, Occurrence, and Health Issues* (F.C. Hawthorne, R. Oberti, G. Della Ventura and A. Mottana, editors). Reviews in Mineralogy & Geochemistry, **67**. Mineralogical Society of America and the Geochemical Society, Chantilly, Virginia, USA.

Hafner, S.S. and Ghose, S. (1971) Iron and magnesium distribution in cummingtonites, $(Fe,Mg)_7Si_8O_{22}(OH)_2$. *Zeitschrift für Kristallographie*, **133**, 301–326.

Hawthorne, F.C. (1978) The crystal structure and site chemistry of fluor-riebeckite. *Canadian Mineralogist*, **16**, 187–194.

Hawthorne, F.C. (1983) The crystal-chemistry of the amphiboles. *Canadian Mineralogist*, **21**, 173–480.

Hawthorne, F.C. and Della Ventura, G. (2007) Short-range order in amphiboles. *Reviews in Mineralogy and Geochemistry*, **67**, 173–222.

Hawthorne, F.C. and Oberti, R. (2007) Amphiboles: Crystal Chemistry. Pp. 1–54 in: *Amphiboles: Crystal Chemistry, Occurrence, and Health Issues* (F.C. Hawthorne, R. Oberti, G. Della Ventura and A. Mottana, editors). Reviews in Mineralogy & Geochemistry, **67**. Mineralogical Society of America and the Geochemical Society, Chantilly, Virginia, USA.

Hawthorne, F.C., Ungaretti, L., Oberti, R., Bottazzi, P. and Czamanske, G.K. (1993) Li: An important component in igneous alkali amphiboles. *American Mineralogist*, **78**, 733–745.

Hawthorne, F.C., Ungaretti, L., Oberti, R., Cannillo, E. and Smelik, E.A. (1994) The mechanism of $^{[6]}$Li incorporation in amphiboles. *American Mineralogist*, **78**, 443–451

Hawthorne, F.C., Oberti, R. and Sardone, N. (1996*a*) Sodium at the A site in clinoamphiboles: the effects of composition on patterns of order. *Canadian Mineralogist*, **34**, 577–593.

Hawthorne, F.C., Della Ventura, G. and Robert., J.L. (1996*b*) Short-range order and long-range order in

https://doi.org/10.1180/minmag.2017.081.064 Published online by Cambridge University Press

amphiboles: A model for the interpretation of infrared spectra in the principal OH-stretching region. *The Geochemical Society, Special Publication* **No. 5.** 49–54.

Hawthorne, F.C., Welch, M.D., Della Ventura, G., Liu, S., Robert, J.L. and Jenkins, D.M. (2000) Short-range order in synthetic aluminous tremolites: An infrared and triple-quantum MAS NMR study. *American Mineralogist*, **85**, 1716–1724.

Iezzi, G., Cámara, F., Della Ventura, G., Oberti, R., Pedrazzi, G. and Robert, J.L. (2004) Synthesis, crystal structure and crystal-chemistry of ferri-clinoholmquistite, $Li_2Mg_3Fe^{3+}_2Si_8O_{22}(OH)_2$. *Physics and Chemistry of Minerals*, **31**, 375–385.

Iezzi, G., Della Ventura, G., Hawthorne, F.C., Pedrazzi, G., Robert, J.-L. and Novembre, D. (2005) The (Mg,Fe^{2+}) substitution in ferri-clinoholmquistite, $\square Li_2\ (Mg,Fe^{2+})_3Fe^{3+}_2Si_8O_{22}(OH)_2$. *European Journal of Mineralogy*, **17**, 733–740.

Ishida, K. (1989) Infrared study of manganoan alkali-calcic amphiboles. *Mineralogical Journal*, **14**, 255–265.

Ishida, K. (1990*a*) Infrared spectra of alkali amphiboles of the glaucophane-riebeckite series and their relation to chemical composition. *Mineralogical Journal*, **15**, 147–161.

Ishida, K. (1990*b*) Identification of infrared OH-librational bands of talc-willemseite solid-solutions and $Al^{(VI)}$-free amphiboles through deuteration. *Mineralogical Journal*, **15**, 93–104.

Ishida, K. (1998) Cation disordering in heat-treated anthophyllites through oxidation and dehydrogenation. *Physics and Chemistry of Minerals*, **25**, 160–167.

Ishida, K., Jenkins, D.M. and Hawthorne., F.C. (2008) Mid-IR bands of synthetic calcic amphiboles of tremolite-pargasite series and of natural calcic amphiboles. *American Mineralogist*, **93**, 1112–1118.

Kloprogge, J.T., Case, M.H. and Frost, R.L. (2001) Raman microscopic study of the Li amphibole holmquistite, from the Martin Marietta Quarry, Bessemer City, NC, USA. *Mineralogical Magazine*, **65**, 775–785.

Krause, L., Herbst-Irmer, R., Sheldrick, G.M. and Stalke, D. (2015) Comparison of silver and molybdenum microfocus X-ray sources for single-crystal structure determination. *Journal of Applied Crystallography*, **48**, 3–10.

Kuzmany, H. (2009) *Solid-state spectroscopy.* Springer, Berlin.

Law, A.D. (1976) A model for the investigation of Hydroxyl spectra of amphiboles. Pp. 677–686 in: *The Physics and Chemistry of Minerals and Rocks* (R.G.J. Strens, editor).

Lazarev, A.N. (1972) *Vibrational Spectra and Structure of Silicates*. Consultants Bureau (Plenum Publishing Company Ltd.), New York, London, 302 pp.

Leissner, L., Schlüter, J., Horn, I. and Mihailova, B. (2015) Exploring the potential of Raman spectroscopy for crystallochemical analyses of complex hydrous silicates: I. Amphiboles. *American Mineralogist*, **100**, 2682–2694.

Lewis, I.R., Chaffin, N.C., Gunter, M.E. and Griffiths, P. R. (1996) Vibrational spectroscopic studies of asbestos and comparison of suitability for remote analysis. *Spectrochimica Acta part A*, **52**, 315–328.

Mustard, J.F. (1992) Chemical analysis of actinolite from reflectance spectra. *American Mineralogist*, **77**, 345–358.

Oberti, R., Hawthorne, F.C., Cannillo, E. and Càmara, F. (2007) Long-range order in amphiboles. Pp. 125–172 in: *Amphiboles: Crystal Chemistry, Occurrence, and Health Issues* (F.C. Hawthorne, R. Oberti, G. Della Ventura and A. Mottana, editors). Reviews in Mineralogy & Geochemistry, **67**. Mineralogical Society of America and the Geochemical Society, Chantilly, Virginia, USA.

Oberti, R., Della Ventura, G., Boiocchi, M., Zanetti, A. and Hawthorne, F.C. (2017) The crystal chemistry of oxo-mangani-leakeite and mangano-mangani-ungarettiite from the Hoskins mine and their apparent but impossible solid-solution – An XRD and FTIR study. *Mineralogical Magazine*, **81**, 707–722.

Paton, C., Hellstrom, J., Paul, B., Woodhead, J. and Hergt, J. (2011) Iolite: Freeware for the visualisation and processing of mass spectrometric data. *Journal of Analytical Atomic Spectrometry*, **26**, 2508–2518.

Rancourt, D.G. and Ping, J.Y. (1991) Voigt-based methods for arbitrary-shape static hyperfine parameter distributions in Mössbauer spectroscopy. *Nuclear Instruments and Methods in Physics Research B*, **58**, 85–97.

Rancourt, D.G., McDonald, A.M., Lalonde, A.E. and Ping, J.Y. (1993) Mössbauer absorber thickness for accurate site populations in Fe-bearing minerals. *American Mineralogist*, **78**, 1–7.

Rancourt, D.G., Ping, J.Y., Boukili, B. and Robert, J.L. (1996) Octahedral-site Fe^{2+} quadrupole splitting distributions from Mössbauer spectroscopy along (OH, F)-annite join. *Physics and Chemistry of Minerals*, **23**, 63–71.

Reece, J.J., Redfern, S.A.T., Welch, M.D., Henderson, C. M.B. and McCammon, C.A. (2002) Temperature-dependent Fe^{2+}–Mn^{2+} order–disorder behaviour in amphiboles. *Physics and Chemistry of Minerals*, **29**, 562 – 570.

Rinaudo, C., Belluso, E. and Gastaldi, D. (2004) Assessment of the use of Raman spectroscopy for the determination of amphibole asbestos. *Mineralogical Magazine*, **68**, 455–465.

Rinaudo, C., Cairo, S., Gastaldi, D., Gianfagna, A., Mazziotti Tagliani, S., Tosi, G. and Conti, C. (2006) Characterization of fluoro-edenite by μ-Raman and μ-

https://doi.org/10.1180/minmag.2017.081.064 Published online by Cambridge University Press

FTIR spectroscopy. *Mineralogical Magazine*, **70**, 291–298.

Robinson, K., Gibbs, G.V. and Ribbe, P.H. (1971) Quadratic elongation: a quantitative measure of distortion in coordination polyhedra. *Science*, **172**, 567–570.

Sheldrick, G.M. (2015) Crystal structure refinement with SHELXL *Acta Crystallographica*, **C71**, 3–8.

Skogby, H. and Rossman, G.R. (1991) The intensity of amphibole OH bands in the infrared absorption spectrum. *Physics and Chemistry of Minerals*, **18**, 64–68.

Strens, R.S.J. (1966) Infrared study of cation ordering and clustering in some (Fe, Mg) amphibole solid solutions. *Chemical Communications*, **519**, 159–520

Wang, A., Dhamelincourt, P. and Turrell, G. (1988*a*) Infrared and low-temperature micro-Raman spectra of the OH stretching vibrations in cummingtonite. *Applied Spectroscopy*, **42**, 1451–1457.

Wang, A., Dhamelincourt, P. and Turrell, G. (1988*b*) Raman microspectroscopic study of the cation distribution in amphiboles. *Applied Spectroscopy*, **42**, 1441–1450.

Zoltai, T. (1981) Amphibole asbestos mineralogy. Pp. 237–278 in: *Amphiboles and other hydrous pyriboles. Mineralogy.* (D.R. Veblen, editor). Reviews in Mineralogy, **9A**. Mineralogical Society of America, Washington DC.

https://doi.org/10.1180/minmag.2017.081.064 Published online by Cambridge University Press